DOI:10.15150/ae.2025.3343



# Parameterization of a stalk structure model for miscanthus based on four-point bending tests

Niklas Bargen-Herzog, Johannes Knapp, Benjamin Kazenwadel, Marcus Geimer

Miscanthus is a renewable energy crop with great potential for use in bioeconomic value chains. A stalk structure model for miscanthus was developed and parameterized using four-point bending tests as a basis for simulative investigations on handling and forming using the discrete element method. The significance of the parameters and their optimum values were identified using Plackett–Burman designs, a subsequent analysis of variance, and the method of steepest ascent. The parameterization obtained enables the essential characteristics of the material behavior observed in the tests to be reproduced in the simulation. The maximum bending force occurring in the simulation deviates by less than 2% from the experimentally determined data.

#### Keywords

Discrete element method (DEM), process simulation, parameter calibration, stalk material, miscanthus

The responsible use of limited resources and the associated expansion of a sustainable energy supply are among the key challenges of our time. Biomass accounted for 47% of the provision of renewable final energy across all sectors (electricity, heat, transport) in Germany in 2024, making it the most important renewable energy source (UMWELTBUNDESAMT 2025). This emphasizes the high relevance of the further development and optimization of bioeconomic value chains.

Miscanthus is a perennial plant native to East Asia with low soil and climate requirements. These properties qualify it as one of the most promising energy crops (FISCHER et al. 2005). In addition to its use as an energetic resource, miscanthus also offers a wide range of material utilization options, for example as a building material or plastic substitute (FRITZ et al. 2009). Today, primarily conventional forage harvesters and balers are used to harvest and compact miscanthus. According to KALTSCHMITT et al. (2009), miscanthus can thus be compacted to a dry matter density of approx. 140 kg m<sup>-3</sup>. Assuming a moisture content of 20% at the time of harvest (MEEHAN et al. 2013), this results in a real density of 175 kg m<sup>-3</sup>. However, due to high transport and storage volumes, the transport and logistics process for miscanthus is currently not economically scalable.

The development of innovative processes and machines is necessary to exploit the potential for energy recovery from energy crops economically. Simulation is an indispensable tool that makes it possible to analyze processes and gain a comprehensive understanding of systems without the cost-intensive construction and operation of test rigs and prototypes. The discrete element method (DEM) has proven to be a suitable simulation method for analyzing material flows. The use of bonding models allows several individual elements to be connected to each other as required, enabling flexible

stalk structures to be modeled and thus processes in agricultural machinery to be analyzed (Becker 2020, JÜNEMANN et al. 2013).

Various stalk structure models are already available for the simulation of stalk-like biomass. Regarding the arrangement of several individual elements to form a stalk, a distinction is made between the three basic structures: chain structure, hollow structure, and full structure. The chain structure is a one-dimensional sequence of individual elements. The hollow structure is made up of several element chains, which are usually arranged in a ring. The full structure is an extension of the hollow structure with at least one additional element chain inside the ring. The majority of existing modeling approaches for stalk material can either be assigned to one of the three structures or represent a hybrid form that combines elements of several structures (JÜNEMANN et al. 2013).

While recent research has paid particular attention to the process simulation of maize (Han et al. 2024, Kovacs et al. 2017, Lenaerts et al. 2014, Wang et al. 2024, Zhang et al. 2020) and straw (Jünemann et al. 2013, Kattenstroth et al. 2011, Liu et al. 2023, Zeng and Chen 2019), there has been a lack of comprehensive studies on the modeling of miscanthus. The number of scientific studies on the material properties of miscanthus has also been limited to date. The few systematic studies on miscanthus include a large-scale field study by Kaack and Schwarz (2001), which provides information on the mechanical properties of miscanthus, including the modulus of elasticity. In addition, research by Miao et al. (2015) and Bargen-Herzog et al. (2024) provides information on the compression behavior of miscanthus.

This work addresses this research gap and deals with four-point bending tests on miscanthus and the subsequent development and parameterization of a stalk structure model for miscanthus. The procedure is based on the multi-stage approach according to Han et al. (2024), which was originally developed for the parameterization of a stalk structure model for maize. Accordingly, material tests, in this case four-point bending tests, form the basis for the development of the stalk structure model. The values of the parameters are assigned using the Plackett-Burman designs, an analysis of variance and the steepest ascent method.

The parameterized stalk structure model enables the simulation of miscanthus processing operations in which the stalks are subjected to bending stress, for example during the round bale wrapping process. Additionally, the investigations are intended to serve as a basis for further research into the simulation of miscanthus and to support the development of innovative machines and processes.

#### Material and Methods

The test material used and the structure of the four-point bending tests are described below. This is followed by a brief introduction to the DEM simulation with a focus on the bonding model used. Finally, the stalk structure model developed for this study is presented and the methodical procedure for its parameterization is shown.

## Test material

The material analyzed was miscanthus plants of the genotype  $Miscanthus \times giganteus$  (Greef and Deuter 1993). Miscanthus is characterized by a segment-like structure of the stalks, which is due to the division of a stalk into nodes and internodes (Figure 1). The diameter and stiffness of the nodes and internodes decrease along the direction of growth, giving miscanthus stems an inhomogeneous

material behavior. This structure is not only found in miscanthus but is a typical feature of many stalk materials.

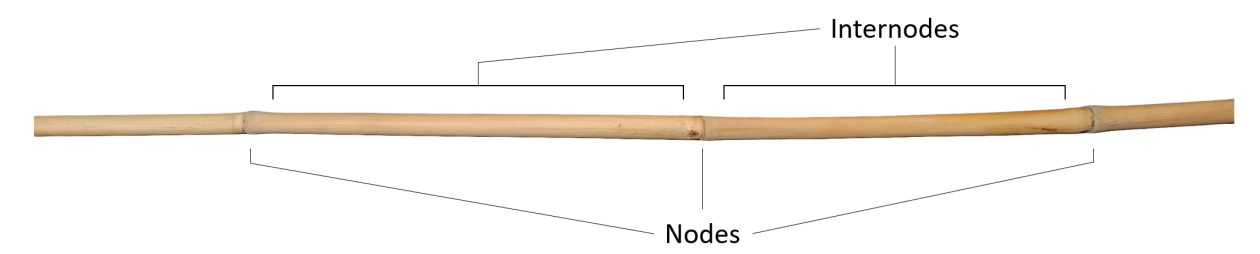


Figure 1: Segmental structure of a miscanthus stalk

Approximately 12 cm long sections of miscanthus stalks, which was cultivated in southern Germany and harvested in spring 2022 and 2023, are used as samples for the material tests. The stalks were stored for several months, minimizing their moisture content so that its influence on the material properties investigated can be assumed to be negligible. A total of 196 samples available were taken independently of their position along the stalk. Due to the inhomogeneous material properties along the direction of growth, the properties of the samples listed in Table 1 reveal correspondingly high coefficients of variation. Since the stalk structure model examined in this study does not represent the inhomogeneities along the stalk, a differentiation according to the sampling position is not subject to the material tests. However, due to the considerable influence of the nodes on the material behavior, a distinction is made between samples with and without nodes. In samples containing a node, the node is always positioned in the center of the sample section.

Table 1: Properties of the miscanthus samples

Quantity	Notation	Arithmetic mean	Standard deviation
Length in mm	I	116.63	15.80
Diameter in mm	d	7.41	1.15
Mass in g	m	1.46	0.70
Density <sup>1)</sup> in kg m <sup>-3</sup>	ρ	274.00	67.00

<sup>1)</sup> The calculation of the density is based on the approximation of a cylindrical volume of the samples.

## Four-point bending test

When handling stalk material, bending stresses occur in many processes, for example in conveying or baling processes. Compared to three-point bending tests, four-point bending tests generate a more uniform bending stress over a defined sample section and thus provide a more representative measurement of the mechanical properties of the heterogeneous stalks. Therefore, four-point bending tests are used as the basis for parameterizing the stalk structure model for miscanthus. The test setup is designed according to the diagram shown in Figure 2. The pressing plunger moves vertically downwards at a constant speed until a bending of 12 mm is reached. This setting is based on preliminary tests in which a drop in power was observed in every case at this displacement. A force sensor records the force applied to the sample via the pressing plunger.

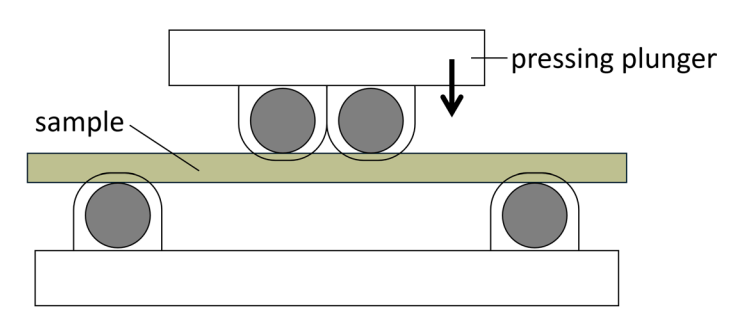


Figure 2: Schematic test setup of the four-point bending tests

#### **DEM-Simulation**

The Altair EDEM software is used to carry out the DEM simulations. For example, bulk material, granular material or culm is modelled in the form of particles or meta-particles (combination of several particles). The environment interacting with the particles is modeled using geometries. The simulation is fundamentally based on the evaluation of Newton's equations of motion. In addition, different contact models are available to describe the interactions between the particles. A basic contact model, which defines how a collision between particles and geometries or between particles themselves takes place, is mandatory. In this study, the Hertz-Mindlin (no slip) model (Cundall and Strack 1979, Hertz 1881, Mindlin 1949, Mindlin and Deresiewicz 1953, Sakaguchi et al. 1993, Tsuji et al. 1992) is used as the basic contact model, as it enables an accurate and efficient calculation of the force.

To combine several individual particles into a meta-particle, it is necessary to use a further contact model to describe particle connections additionally to the basic contact model. The Bonding V2 model, which is based on the work of Potyondy and Cundall (2004), is used for this purpose. The connections between the particles are generated at a specified time (creation time). The forces in the normal and tangential directions ( $F_n$ ,  $F_t$ ) are set to zero and calculated incrementally for each time step according to Equations 1 and 2. The force difference per time step ( $\delta F_n$ ,  $\delta F_t$ ) thus results from the product of the velocity ( $v_n$ ,  $v_t$ ), the normal or shear stiffness ( $S_n$ ,  $S_t$ ), the contact area (A) and the time step ( $\delta t$ ). Normal stiffness and shear stiffness refer to the stiffness per unit area and are therefore specified in the unit N m<sup>-3</sup>. Similarly, the moments ( $M_n$ ,  $M_t$ ) are calculated using the angular velocity ( $w_n$ ,  $w_t$ ) and the moment of inertia (I) according to Equations 3 and 4. The bond radius (I) is used to calculate the contact area (Equation 5) and the moment of inertia (Equation 6). It is defined as the product of the smallest particle radius of a contact pair (I) and the scaling factor Bonded Disk Scale (I) (Han et al. 2024).

$$\delta F_{\rm n} = -v_{\rm n} S_{\rm n} A \delta t \tag{Eq. 1}$$

$$\delta F_{t} = -v_{t} S_{t} A \delta t \tag{Eq. 2}$$

$$\delta M_{\rm n} = -w_{\rm n} S_{\rm t} I \delta t \tag{Eq. 3}$$

$$\delta M_{\rm t} = -w_{\rm t} S_{\rm n} \frac{J}{2} \delta t \tag{Eq. 4}$$

with

$$A = \pi R_{\rm B}^{2} \tag{Eq. 5}$$

$$J = \frac{1}{2}\pi R_{\rm B}^{4}$$
 (Eq. 6)

$$R_{\rm B} = R_{\rm min} * BDS \tag{Eq. 7}$$

A bond between particles lasts until the normal and tangential shear stresses exceed specified maximum values ( $\sigma_{\text{max}}$ ,  $\tau_{\text{max}}$ ). These threshold values are calculated according to Equations 8 and 9 (Han et al. 2024).

$$\sigma_{\text{max}} < \frac{-F_{\text{n}}}{A} + \frac{2M_{\text{t}}}{I} R_{\text{B}} \tag{Eq. 8}$$

$$\tau_{\text{max}} < \frac{-F_{\text{t}}}{A} + \frac{M_{\text{n}}}{I} R_{\text{B}} \tag{Eq. 9}$$

## Stalk structure model for miscanthus

The stalk structure model for miscanthus used in this study is a combination of the hollow and full structure. The hollow structure models the internodes, while the full structure reflects the woody nature of the nodes. In both the hollow and full structure, twelve elements are distributed flush around the circumference of a circle. In addition, the full structure contains a 13th element inside the particle circle (Figure 3). A miscanthus stalk is thus described by a meta-particle composed of three different types of particles: elements representing the internodes (*type A*), elements representing the node rings (*type B*) and elements representing the node center (*type C*).

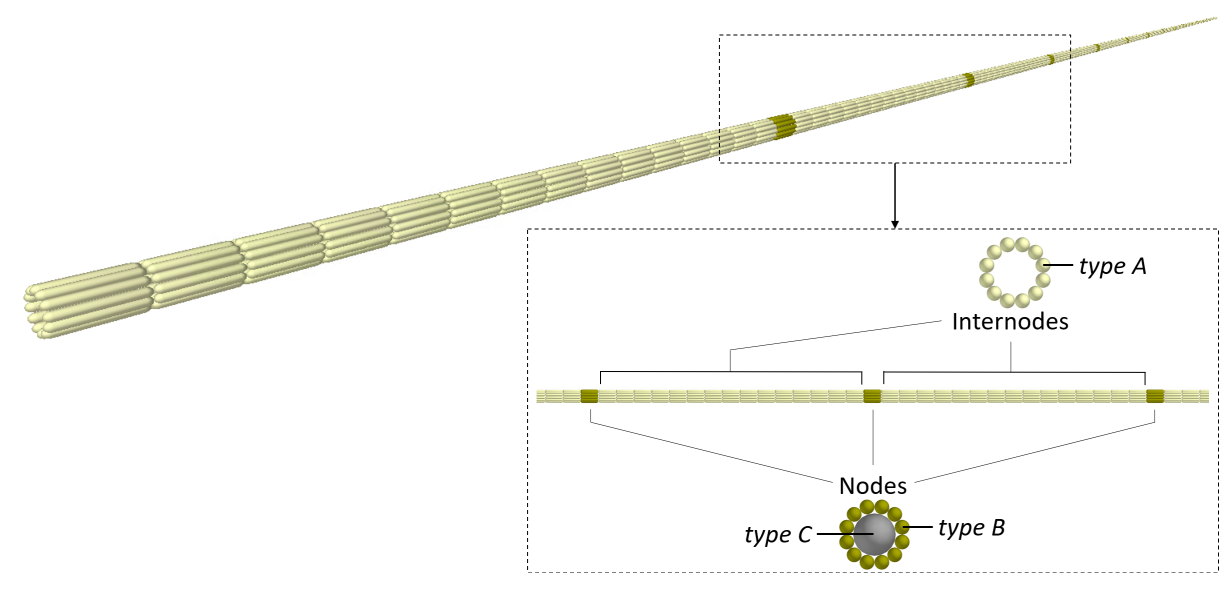


Figure 3: Stalk structure model for miscanthus

All elements used are sphero-cylindrical bodies. These are often used for modeling stalk material, as fewer elements are required to represent a stalk of the same length compared to spherical elements. With an increasing number of elements and thus more motion and contact equations to be solved, the computing resources required increase significantly. On the other hand, there is a risk of no longer achieving the desired level of detail with fewer and, consequently, larger elements. Taking this conflict of objectives into account, a length of 10 mm is selected for each of the spherical cylinders in this stalk structure model, so that a stalk with a length of 2,500 mm is composed of 250 ring structures. Thereby, 15 hollow ring structures to simulate an internode and one filled ring structure to simulate a node are arranged alternately.

The diameters of the spherocylinders are derived from the specifications that the total diameter of the internodes is 7.5 mm and the total diameter of a node is 7.7 mm (Table 2). The density of the elements results from the finding that samples without nodes have an average density of 254 kg m<sup>-3</sup> and samples with nodes have an average density of 289 kg m<sup>-3</sup>. Due to the hollow structure of the stalks, this results in the values given in Table 2.

Quantity	Notation	Spherocylinder for modeling the internodes	Spherocylinder for modeling the node ring	Spherocylinder for modeling the node center
Length in mm	I	10.00	10.00	10.00
Diameter in mm	d	1.54	1.58	4.53
Density in kg m <sup>-3</sup>	ρ	527.87	785.51	785.51

#### Parameterization of the stalk structure model

The use of the stalk structure model in the DEM simulation requires the definition of several parameters from different categories. Firstly, the material properties of the internodes and the nodes, which are characterized by the Poisson's ratio and the Young's modulus, are to be defined. Secondly, the impact coefficient and static and dynamic friction coefficients for modeling the interactions between the materials (internodes, nodes, steel) are to be determined. This includes the interaction between identical materials (e.g. internodes-internodes) as well as between different material pairings (e.g. internodes-nodes, internodes-steel). Thirdly, the model includes parameters to describe the bonding V2 model. These parameters are the normal and shear stiffness, the critical load in normal and shear direction and the bonded disc radius. These parameters must be specified for connections of internode elements with each other, of node elements with each other and of internode elements with node elements.

The parametrization of the stalk structure model is based on the results of the four-point bending tests and their representation in the simulation. Since the miscanthus samples analyzed in the tests are not whole stalks, but only segments, the replication of the samples in the simulation represents a 110 mm long section of the described stalk structure model. While the model of a miscanthus sample without nodes (Figure 4) is composed exclusively of the elements for modeling an internode, the replication of a miscanthus sample with node (Figure 5) contains the filled ring structure in the middle position which is characteristic of a node.

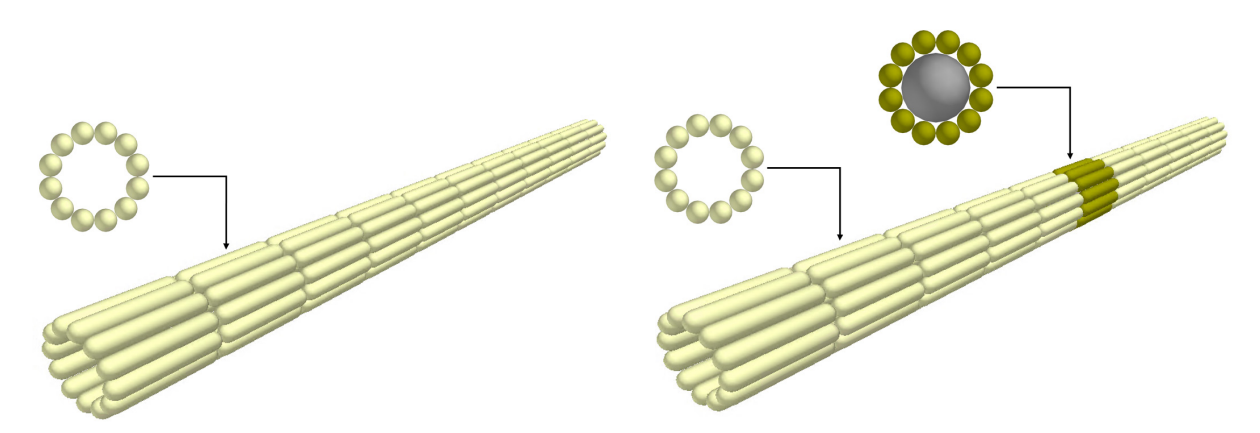


Figure 4: Model of a sample without nodes

Figure 5: Model of a sample with node

In the first step, the bending behavior of samples without nodes is evaluated, so that initially only the parameters for describing the material of the internodes and their interactions with steel and themselves have to be taken into account. Once these parameters have been defined, the tests with the samples with node are also used to parameterize the material of the nodes and their interactions.

Despite this two-stage approach to parameterization, many parameters need to be evaluated in both stages. To identify the parameters with the greatest influence on the simulation result, it is advisable to use Plackett–Burman designs. These test plans are based on defining a low level and a high level for the parameters to be analyzed and switching between these values according to a predefined scheme. In the plans, the number -1 stands for low level and the number 1 for high level. In this way, it is possible to analyze a number of n-1 parameters with n simulation runs and to discover the significant parameters with the help of a variance analysis. Plackett–Burman designs are available for 8 to 96 test runs, whereby the number of tests must be a multiple of 4 (SIEBERTZ et al. 2017).

Table 3 lists the parameters and the corresponding low level and high level values that are relevant for the replication of the miscanthus samples without nodes. Table 4 shows the equivalent for miscanthus samples with node. Regarding the modeling of samples without nodes, the influence of 13 parameters is analyzed. The parameter setting identified to describe the internodes is adopted for the modeling of the samples with nodes and, based on this, 12 further parameters are investigated. In both cases, 16 simulation runs are required using the Plackett–Burman designs. Since up to 15 factors can be assigned to these plans, two respectively three columns remain vacant and are filled by dummy variables.

Table 3: Relevant parameters with low and high level for the modeling of miscanthus samples without nodes

Parameter	Material	Notation	Low Level (-1)	High Level (+1)
Poisson's Ratio	Internode	$v_{\mathrm{I}}$	0.15	0.45
Young's Modulus in Pa	Internode	$E_{\mathrm{I}}$	2 · 10 <sup>9</sup>	6 · 10 <sup>9</sup>
Coefficient of Restitution	Internode-Steel	$e_{\mathrm{I-St}}$	0.2	0.6
Coefficient of Static Friction	Internode-Steel	$\mu_{\text{S,I-St}}$	0.2	0.6
Coefficient of Rolling Friction	Internode-Steel	$\mu_{ m R,I-St}$	0.1	0.3
Coefficient of Restitution	Internode-Internode	$e_{\mathrm{I-I}}$	0.2	0.6
Coefficient of Static Friction	Internode-Internode	$\mu_{\mathrm{S,I-I}}$	0.2	0.6
Coefficient of Rolling Friction	Internode-Internode	$\mu_{\mathrm{R,I-I}}$	0.1	0.3
Normal Stiffness in Nm <sup>-3</sup>	Internode-Internode	$S_{N,I-I}$	5 · 10 <sup>10</sup>	25·10 <sup>10</sup>
Shear Stiffness in Nm <sup>-3</sup>	Internode-Internode	$S_{T,I-I}$	2·10 <sup>10</sup>	10·10 <sup>10</sup>
Max. Normal Strength in Pa	Internode-Internode	$\sigma_{ m max,I-I}$	5 · 10 <sup>7</sup>	25 · 10 <sup>7</sup>
Max. Shear Strength in Pa	Internode-Internode	$ au_{ m max,I-I}$	2 · 10 <sup>7</sup>	10 · 10 <sup>7</sup>
Bonded Disk Scale	Internode-Internode	$BDS_{I-I}$	0.9	1.8
Dummy Variables	-	А, В	-	-

Table 4: Relevant parameters with low and high level for the modeling of miscanthus samples with node

Parameter	Material	Notation	Low Level (-1)	High Level (+1)
Poisson's Ratio	Node	$v_{ m N}$	0.15	0.45
Young's Modulus in Pa	Node	$E_{ m N}$	3 · 10 <sup>9</sup>	9 · 10 <sup>9</sup>
Normal Stiffness per unit area in Nm <sup>-3</sup>	Internode-Node	$S_{N,I-N}$	5·10 <sup>10</sup>	20·10 <sup>10</sup>
Shear Stiffness per unit area in Nm <sup>-3</sup>	Internode-Node	$S_{T,I-N}$	2·10 <sup>10</sup>	10·10 <sup>10</sup>
Normal Strength in Pa	Internode-Node	$\sigma_{ m max,I-N}$	2 · 10 <sup>7</sup>	10 · 10 <sup>7</sup>
Shear Strength in Pa	Internode-Node	$ au_{ ext{max,I-N}}$	1 · 10 <sup>7</sup>	5 · 10 <sup>7</sup>
Bonded Disk Scale	Internode-Node	$BDS_{I-N}$	0.9	1.8
Normal Stiffness in Nm <sup>-3</sup>	Node-Node	$S_{N,N-N}$	10·10 <sup>10</sup>	50·10 <sup>10</sup>
Shear Stiffness in Nm <sup>-3</sup>	Node-Node	$S_{T,N-N}$	4·10 <sup>10</sup>	20·10 <sup>10</sup>
Max. Normal Strength in Pa	Node-Node	$\sigma_{ m max,N-N}$	10 · 10 <sup>7</sup>	50 · 10 <sup>7</sup>
Max. Shear Strength in Pa	Node-Node	$ au_{ m max,N-N}$	4 · 10 <sup>7</sup>	20 · 10 <sup>7</sup>
Bonded Disk Scale	Node-Node	$BDS_{N-N}$	0.9	1.8
Dummy Variables	-	C, D, E	-	-

The determination of the low level and high level values is based on various research studies on miscanthus and other stalk-like materials. Specific research has already been carried out on the Poisson's ratio (MIAO et al. 2015) and the Young's modulus (KAACK and SCHWARZ 2001, LIU and Koc 2017, LIU et al. 2012) for miscanthus. With regard to the description of the material interactions of miscanthus, there is currently a lack of well-founded data, so that studies on other stalk materials, especially maize, are used as a benchmark (HAN et al. 2024, Kovács et al. 2015, LI et al. 2024, LIU et al. 2023, ZHANG et al. 2020).

The simulation runs according to the Plackett-Burman design are analyzed in the form of an analysis of variance following Siebertz et al. (2017). This is based on defining a key performance indicator (y) that is characteristic of the phenomenon to be analyzed.

To determine the total variance of the simulation series  $V_{\rm Ges}$  (Equation 10), first the mean value  $\bar{y}$  of the n trials is determined and then the deviation of the values of the individual trials  $y_{\rm i}$  from the mean value  $\bar{y}$  is considered.

$$V_{\text{Ges}} = \frac{1}{n} \sum_{i=1}^{n} (y_i - \bar{y})^2$$
 (Eq. 10)

In addition to the total variance of the test series, a partial variance  $V_j$  is assigned to each parameter (Equation 12). This results from the effect of a parameter  $E_j$ , which is calculated by the mean values of all simulation runs with the low value  $\bar{y}_{j,-}$  and the mean value of all simulation runs with the high value  $\bar{y}_{i,+}$  (Equation 11).

$$E_j = \frac{\bar{y}_{j,+} - \bar{y}_{j,-}}{2}$$
 (Eq. 11)

$$V_j = E_j^2 \tag{Eq. 12}$$

To describe the uncertainty in determining the effects, the standard error S is calculated from the effects of the dummy variables  $E_{\mathrm{DV},i}$  according to Equation 13, where  $n_{\mathrm{DV}}$  indicates the number of dummy variables.

$$S = \frac{1}{n_{\rm DV}} \sum_{i=1}^{n_{\rm DV}} E_{{\rm DV},i}$$
 (Eq. 13)

Finally, the t-statistic is derived by dividing the effects by the standard error (Equation 14). In general, a higher t-value  $t_j$  indicates a greater significance of the parameter. The critical t-value  $t_{\rm crit}$ , which depends on the number of degrees of freedom and the specified probability of error, serves as the threshold value. With 15 degrees of freedom and a probability of error of 5%, the critical t-value is 2.13 (Klein 2021). In this study, parameters with a t-value greater than the critical t-value are classified as significant and used for the further parameterization of the simulation model.

$$t_j = \frac{E_j}{S} \tag{Eq. 14}$$

Further parameterization is carried out using the method of steepest ascent. In an iterative procedure, the parameters with the greatest effect are systematically varied, whereby the direction is determined by the sign of the effect. The step size is first selected in such a way that the entire parameter space between the low level and the high level value is considered in five steps. The simulation plan is then continued with a smaller step size, starting from the simulation in which the key performance indicator has the next smallest value to the target value measured in the tests. The step size of the parameters is set to a tenth of the previously used step size. In addition, the simulations are now carried out twice and an average value of the key performance indicator is calculated to reduce the influence of small variations in the simulation. The parameters are varied until the target value is

exceeded for the first time. The simulation run that best approximates the target value is run a third time for verification.

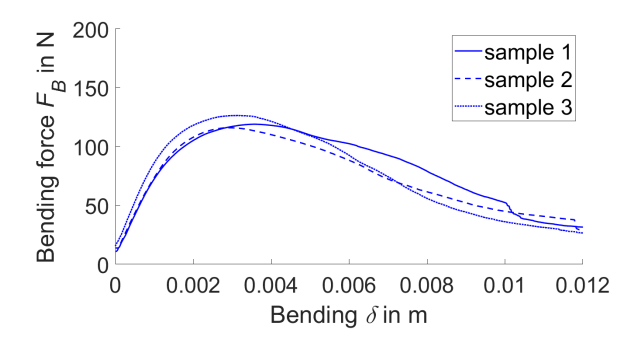
## Results

The results include the evaluation of the experimental four-point bending tests on the one hand and the parameterization of the stalk structure model on the other. The latter is divided into the parameterization of the internodes and the parameterization of the nodes.

## Results of the four-point bending tests

The material tests carried out include 40 four-point bending tests. These four-point bending tests are used for the parameterization of the stalk structure model. In the four-point bending tests, 20 samples with and 20 samples without nodes were examined. It was observed that samples without nodes primarily exhibited plastic deformation in the form of slight buckling without visible signs of breakage. In contrast, samples with node showed a pronounced failure behavior, which manifested itself in the breakage of individual fibers on the convex side of the bend. The fibers on the concave side did not tear apart and thus prevented complete separation of the stem. These differences in deformation and failure behavior suggest that internodes and nodes have different mechanical properties and interactions with each other.

The characteristic differences between the two sample types under bending load described above can also be seen in the curve of the bending force over the deflection. Figure 6 and Figure 7 show examples of the curve of the bending force for three samples without nodes and three samples with nodes. The abrupt drop in force, which only occurs in the curves of the samples with node, indicates a fracture of individual or several fibers.



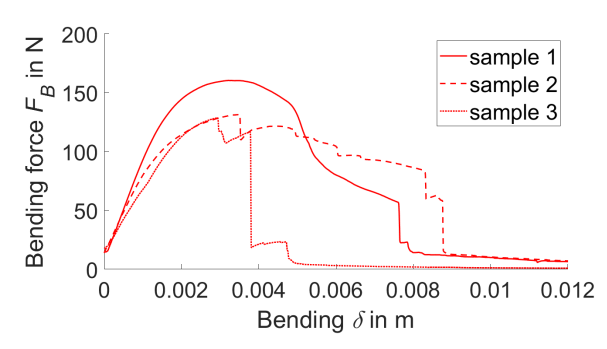


Figure 6: Bending force-deflection curve for three exemplary samples without nodes

Figure 7: Bending force-deflection curve for three exemplary samples with node

The maximum bending force is used as a quantitative value to describe the four-point bending tests. Table 5 shows the mean value of the maximum bending force for all tests, as well as the mean values separately for the tests using samples without nodes and samples with node. The standard deviation, which is also given in Table 5, indicates a large spread of the measured values. This is due to the inhomogeneous material properties of miscanthus, which were not examined in detail in this study.

Table 5: Results of the four-point bending tests

Samples	Number of samples	Mean value of the max. bending force $F_{\rm B}$ in N	Standard deviation in N
All samples	40	142.55	78.32
Samples without nodes	20	134.45	69.54
Samples with node	20	150.64	85.46

## Parameterization of the internodes

The parameterization of the internodes is based on the modeling of the four-point bending tests of the miscanthus samples without nodes. According to the Plackett-Burman design, 16 simulations are carried out. In the process, 13 parameters are considered, each of which can assume the values low level (-1) and high level (1). The results of the simulations are documented in the form of the maximum bending force  $F_B$  and are shown together with the simulation plan in Table A1 in the Appendix.

The analysis of variance, the detailed results of which are listed in Table 6, clearly shows the influence of the parameters investigated. The total variance of the system is 5,960 N<sup>2</sup>. The largest partial variance of 1,915 N<sup>2</sup> is attributed to the bonded disk scale ( $BDS_{I-I}$ ) and leads to a t-value of 4.28. The bonded disk scale is therefore the parameter with the greatest significance. With t-values greater than 2.13, the normal stiffness ( $S_{N,I-I}$ ), the coefficient of rolling friction between the internodes ( $\mu_{R,I-I}$ ) and the coefficient of restitution between internodes and steel ( $e_{I-St}$ ) are also classified as significant.

Table 6: Analysis of variance of the Plackett-Burman simulation results of the miscanthus samples without nodes

Parameter	Mean value (−1) in N	Mean value (+1) in N	Effect in N	Partial variance in N <sup>2</sup>	t-value
$v_{\rm I}$	89.44	68.05	-10.70	114.44	-1.05
$E_{\mathrm{I}}$	66.82	90.67	11.93	142.23	1.17
$e_{\mathrm{I-St}}$	54.25	103.24	24.49	599.95	2.39
$\mu_{S,I-St}$	69.79	87.70	8.95	80.19	0.88
$\mu_{ m R,I-St}$	83.82	73.68	-5.07	25.71	-0.50
$e_{\mathrm{I-I}}$	69.24	88.25	9.50	90.31	0.93
$\mu_{S,I-I}$	73.67	83.82	5.08	25.78	0.50
$\mu_{\mathrm{R,I-I}}$	106.49	51.00	-27.75	769.79	-2.71
$S_{N,I-I}$	41.68	115.81	37.06	1,373.80	3.62
$S_{T,I-I}$	97.66	59.83	-18.92	357.81	-1.85
$\sigma_{ m max,I-I}$	86.23	71.26	-7.48	56.01	-0.73
$ au_{ ext{max,I-I}}$	64.62	92.87	14.12	199.47	1.38
$BDS_{I-I}$	34.98	122.51	43.76	1,915.22	4.28

All parameters that are not significant according to the analysis of variance are assigned the mean value between their low level and high level value for further consideration. The four parameters classified as significant are varied according to the method of steepest ascent as shown in Table 7. The expectation that the maximum bending force increases in the ascending direction of the parameters is confirmed. The real test results are best reproduced using the value assignments according to number 8 of the simulation plan. Three simulation runs with these settings result in an average value of the maximum bending force of 133.20 N. Compared to the mean value of the 4-point bending test of 134.45 N, this corresponds to a percentage deviation of 0.93%.

Table 7: Simulation plan and results according to the method of steepest ascent for samples without nodes

No.	Coef. of Restitution $e_{\text{I-St}}$	Coef. of Rolling Friction $\mu_{\text{R,I-I}}$	Normal Stiffness $S_{ m N,I-I}$ in Nm $^{-3}$	Bonded Disk Scale BDS <sub>I-I</sub>	Bending force $F_{\mathrm{B}}$ in N
1	0.2	0.30	5·10 <sup>10</sup>	0.900	13.99
2	0.3	0.25	10·10 <sup>10</sup>	1.125	41.11
3	0.4	0.20	15·10 <sup>10</sup>	1.350	105.13
4	0.5	0.15	20·10 <sup>10</sup>	1.575	217.06
5	0.6	0.10	25·10 <sup>10</sup>	1.800	398.03
6	0.41	0.195	15.5 · 10 <sup>10</sup>	1.3725	92.58 <sup>1)</sup>
7	0.42	0.190	16.0 · 10 <sup>10</sup>	1.3950	120.55 <sup>1)</sup>
8	0.43	0.185	16.5 · 10 <sup>10</sup>	1.4175	133.20 <sup>2)</sup>
9	0.44	0.180	17.0 · 10 <sup>10</sup>	1.4400	159.66 <sup>1)</sup>

<sup>1)</sup> Mean value of 2 simulation runs.

 $<sup>^{2)}</sup>$  Mean value of 3 simulation runs.

#### Parameterization of the nodes

The four-point bending tests of the miscanthus samples with node are used to parameterize the nodes. The parameters for describing the material of the internodes are known from the previous step and are adopted in this configuration. In addition, the assumption is made that, on the one hand, the determined impact coefficient and the determined friction coefficients between internodes and steel also apply to the material pairing of nodes and steel (Equations 15–17). On the other hand, the parameters for describing the impact and friction behavior between internodes are also adopted for the interactions between internodes and nodes, as well as between nodes (Equations 18–20).

$$e_{I-St} = e_{N-St} \tag{Eq. 15}$$

$$\mu_{S,I-St} = \mu_{S,N-St} \tag{Eq. 16}$$

$$\mu_{R,I-St} = \mu_{R,N-St} \tag{Eq. 17}$$

$$e_{I-I} = e_{I-N} = e_{N-N}$$
 (Eq. 18)

$$\mu_{S,I-I} = \mu_{S,I-N} = \mu_{S,N-N}$$
 (Eq. 19)

$$\mu_{R,I-I} = \mu_{R,I-N} = \mu_{R,N-N}$$
 (Eq. 20)

Consequently, twelve parameters remain, which are analyzed using the Plackett-Burman design. The simulation plan and the associated results are listed in Table A2 in the Appendix. The analysis of variance (Table 8) results in a total variance of 2,803.38  $\rm N^2$ . Only the bonded disk scale ( $BDS_{\rm I-N}$ ) and the normal stiffness ( $S_{\rm N,I-I}$ ), which characterize the connection between internodes and nodes, exceed the critical t-value of 2.13. The other parameters are not considered significant and are defined as the mean value between their low level and high level value. Deviating from this, the maximum bending stress between internodes and nodes ( $\sigma_{\rm max,I-N}$ ) is assigned its high level value. This is due to the observation that in all eight simulation runs with assignment of the low level value, the sample breaks completely, while in the eight simulations using the high level value, only individual fibers break. The latter represents the material behavior observed in the tests much more accurately.

Table 8: Analysis of variance of the Plackett-Burman simulation results of the miscanthus samples with node

Parameter	Mean value (−1) in N	Mean value (+1) in N	Effect in N	Partial variance in N <sup>2</sup>	t-value
$v_{\rm N}$	87.61	91.83	2.11	4.46	0.42
$E_{\rm N}$	93.55	85.88	-3.83	14.68	-0.77
$S_{N,I-N}$	59.61	119.83	30.11	906.63	6.06
$S_{T,I-N}$	91.77	87.66	-2.06	4.23	-0.41
$\sigma_{ m max,I-N}$	86.55	92.88	3.16	10.00	0.64
$ au_{ m max,I-N}$	84.35	95.08	5.36	28.76	1.08
$BDS_{I-N}$	50.26	129.17	39.46	1,556.91	7.94
$S_{N,N-N}$	85.38	94.05	4.34	18.81	0.87
$S_{T,N-N}$	91.69	87.74	-1.97	3.90	-0.40
$\sigma_{ m max,N-N}$	94.88	84.55	-5.16	26.65	-1.04
$ au_{ m max,N-N}$	93.58	85.85	-3.87	14.96	-0.78
$BDS_{N-N}$	85.66	93.77	4.05	16.43	0.82

In this case, the method of steep ascent is based only on the variation of two parameters. Again, the expectation that the maximum bending force increases in an ascending direction is confirmed. The best approximation of the test results is achieved by the parameter settings of simulation number 10 (Table 9). The mean value of the maximum bending force of three simulation runs with these settings is 147.80 N and thus deviates by 1.89% from the corresponding value of the tests (150.64 N).

Table 9: Simulation plan and results according to the method of steepest ascent for samples with node

Nr.	Normal Stiffness $S_{ m N,I-N}$ in Nm $^{-3}$	Bonded Disk Scale $BDS_{\mathrm{I-N}}$	Bending force $F_{ m B}$ in N
1	5.00 · 10 <sup>10</sup>	0.900	22.45
2	8.75 · 10 <sup>10</sup>	1.125	58.77
3	12.50 · 10 <sup>10</sup>	1.350	118.74
4	16.25 · 10 <sup>10</sup>	1.575	169.08
5	20.00 · 10 <sup>10</sup>	1.800	174.32
6	12.875 · 10 <sup>10</sup>	1.3725	128.46 <sup>1)</sup>
7	13.250 · 10 <sup>10</sup>	1.3950	134.47 <sup>1)</sup>
8	13.625 · 10 <sup>10</sup>	1.4175	139.94 <sup>1)</sup>
9	14.000 · 10 <sup>10</sup>	1.4400	142.30 <sup>1)</sup>
10	14.375 · 10 <sup>10</sup>	1.4628	147.80 <sup>2)</sup>
11	14.750 · 10 <sup>10</sup>	1.4850	155.67 <sup>1)</sup>

<sup>1)</sup> Mean value of 2 simulation runs.

Table A3 in the Appendix provides an overview of the values identified in this study for the parameterization of the stalk structure model of miscanthus.

<sup>2)</sup> Mean value of 3 simulation runs.

## Discussion

The differences in the deformation behavior of samples without nodes and samples with node are not only evident in the experimental tests but also occur in the simulation. Figure 8 compares the simulation results of a sample without nodes with the simulation results of a sample with node. In the case without nodes, the fibers are compressed and the connections between the individual elements remain largely intact. In the case of the samples with nodes, however, the particle connections on the convex side between the nodes and internodes break apart under load. On the concave side, the connections remain intact and prevent the sample from breaking completely.

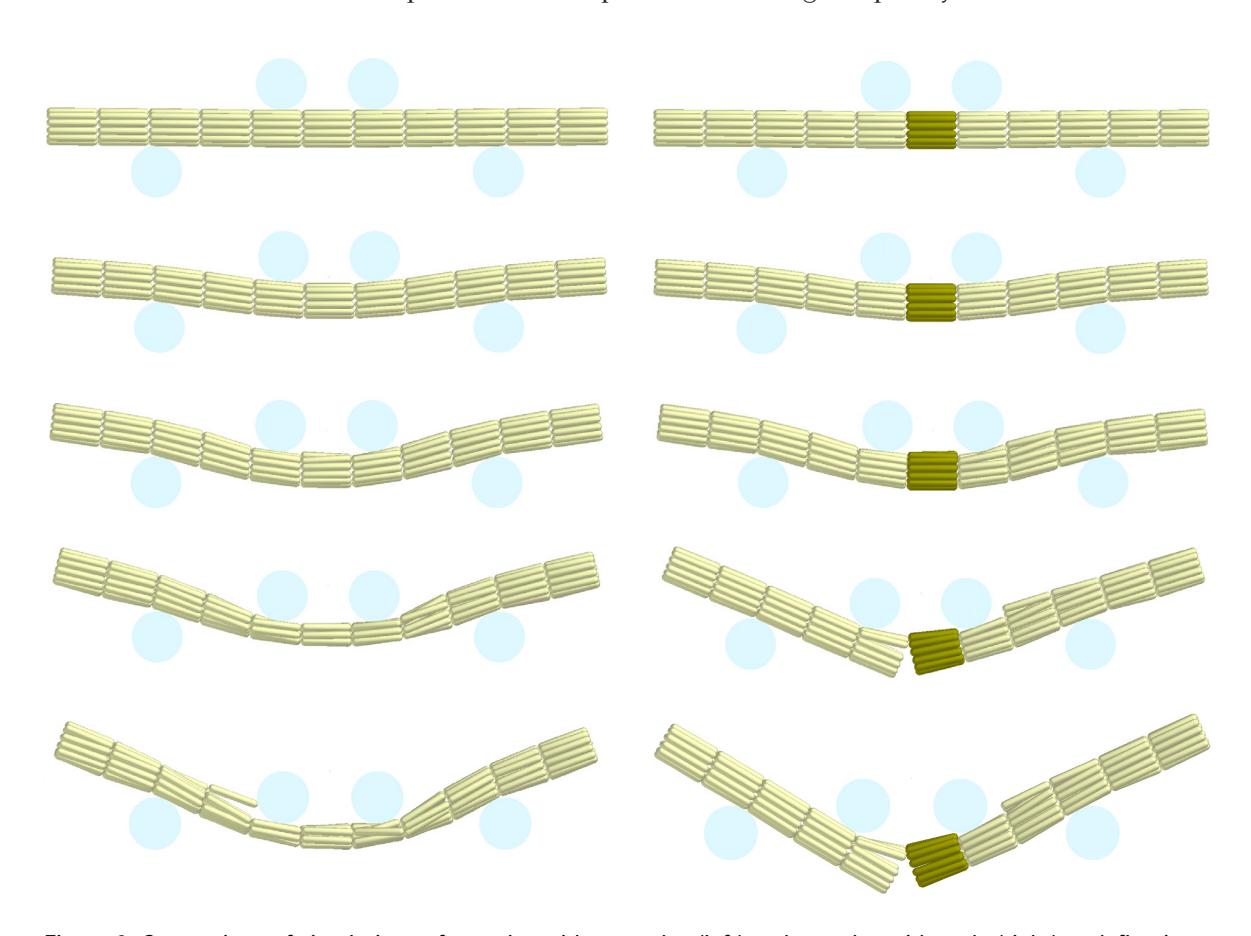
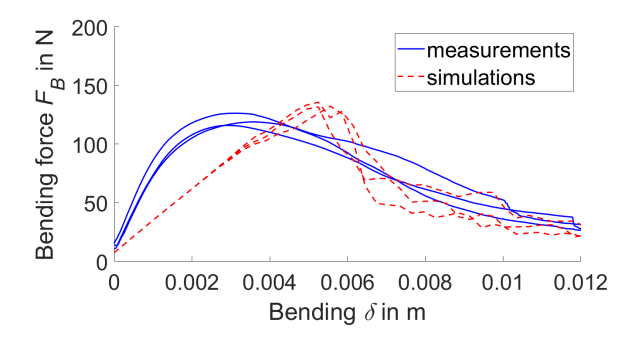


Figure 8: Comparison of simulations of samples without nodes (left) and samples with node (right) at deflections of 0 mm, 3 mm, 6 mm, 9 mm and 12 mm (from top to bottom)

Figure 9 and Figure 10 each contain the results of three simulation runs and three exemplary measurements. Figure 9 shows the results for samples without nodes, while Figure 10 displays the results for samples with node. Both the measurements and the simulations show abrupt drops in force for the samples with node, which are characteristic of the breakage of individual fibers visible in Figure 8. In contrast, no abrupt drops are recognizable in the curves for the samples without nodes. Thus, an essential characteristic of the deformation behavior of miscanthus can be represented in the simulation.

However, the diagrams also show that in both cases the bending force in the simulation initially increases more slowly than in the experiments. As a result, the maximum bending force is reached at a larger deflection. This discrepancy between simulation and reality is because the parameterization

of the stalk structure model is only based on the evaluation of the maximum bending force and not on the curve of the bending force.



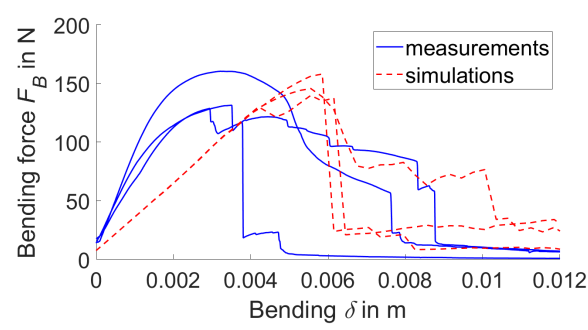


Figure 9: Bending force-deflection curve for three measurements and simulations of samples without nodes

Figure 10: Bending force-deflection curve for three measurements and simulations of samples with node

The stalk structure model of miscanthus used in this study does not take into account the inhomogeneous material properties within a miscanthus stalk. Instead, the material behavior corresponding to the average of a stalk is assumed for all internodes and nodes of a culm. For this reason, no differentiation was made between the samples of the four-point bending tests with regard to their position on the culm. A more differentiated test evaluation, in which the position of the samples is taken into account, opens up the possibility of assigning individual material properties to each segment and, based on this, creating a more precise stalk structure model of miscanthus.

Another aspect that influences the accuracy of the stalk structure model is the discretization of a stalk into individual elements. A finer discretization, in which a stalk is divided into more individual elements, can increase the accuracy of the simulation. However, the increased level of detail is directly related to the computational resources required. The right balance between model accuracy and computational effort is therefore a critical factor to consider when creating a stalk structure model. The discretization used in this study has proven to be suitable for mapping the main phenomena of the four-point bending test. For the analysis of other applications, an individual assessment of the tradeoff between level of detail and computational effort must be made.

## **Conclusions**

As a basis for the development and parameterization of a stalk structure model for miscanthus, four-point bending tests were carried out and evaluated. Significant differences in the material behavior of internodes and nodes were evident. It was found that miscanthus tends to break at the transition point between nodes and internodes under load. The maximum bending force in four-point bending tests of miscanthus samples without nodes was 134.45 N on average. In contrast, a value of 150.64 N was determined for miscanthus samples with node.

To account for the discrepancy between internodes and nodes, internodes and nodes were simulated in the stalk structure model using different materials and structures. The internodes are composed of spherocylindrical elements with a length of 10 mm and a diameter of 1.54 mm. An internode comprises 15 hollow structures arranged in a row, each consisting of twelve elements arranged in a circle.

A node consists of a total of 13 spherocylindrical elements, each of which has a length of 10 mm. A larger element with a diameter of 4.54 mm is encased in a circle by twelve smaller elements with a diameter of 1.58 mm.

To parameterize the model, initially only the material of the internodes was considered. For this purpose, the stalk structure model of miscanthus was limited to a section corresponding to a miscanthus sample without nodes. Based on 16 simulation runs according to the Plackett-Burman design, the bonded disk scale (BDS<sub>I-I</sub>), the normal stiffness (S<sub>NI-I</sub>), the coefficient of rolling friction between the internodes ( $\mu_{RI-I}$ ) and the coefficient of restitution between internodes and steel ( $e_{I-St}$ ) were identified as significant parameters by the analysis of variance. Suitable values for these parameters were determined using the method of steepest ascent, so that the deviation between simulation and tests in terms of the maximum bending force occurring was 0.93%.

Miscanthus samples with nodes were then considered to describe the material behavior of the nodes and their interactions with the internodes. The parameterization was carried out in analogy to the process used for the internodes. The bonded disk scale (BDS $_{I-I}$ ) and the normal stiffness (S $_{NI-I}$ ), both related to the connection between nodes and internodes, were found to be significant parameters. Using the final parameterization, the maximum bending force occurring in the simulation deviates by 1.89% from the value determined in the tests.

The stalk structure model presented in this article and the identified model parameters serve as a basis for the simulation of miscanthus. In further research, it must be examined to what extent the stalk structure model and the parameterization based on the four-point bending tests are suitable for reflecting the material behavior of miscanthus even under deviating load types.

## References

- Bargen-Herzog, N.; Knapp, J.; Geimer, M. (2024): Empirical determination of the compression behaviour of miscanthus round bales. In: AgEng2024, Agricultural Engineering challenges in existing and new agroecosystems, EurAgEng, 1–4 July 2024 in Athens, Greece, pp. 1065–1072, https://doi.org/10.5445/IR/1000173525
- Becker, A. (2020): Herausforderungen an die moderne Diskrete Elemente Methode (DEM) für die Simulation landwirtschaftlicher Güter. In: SIMULAND 2020: Simulation landtechnischer Prozesse, Hg. Jahr, A.; Batos, A., Hochschule Düsseldorf, S. 65–92
- Cundall, P.A.; Strack, O.D.L. (1979): A discrete numerical model for granular assemblies. Géotechnique 29, pp. 47–65, https://doi.org/10.1680/geot.1979.29.1.47
- Fritz, M.; Formowitz, B.; Eppel-Hotz, A.; Jodl, S.; Kuhn, W. (2009): Miscanthus: Anbau und Nutzung (No. 19), Berichte aus dem TFZ. Technologie- und Förderzentrum im Kompetenzzentrum für Nachwachsende Rohstoffe, Straubing. https://www.tfz.bayern.de/mam/cms08/rohstoffpflanzen/dateien/bericht\_19\_gesch\_tzt.pdf, accessed on 28 Aug 2025
- Greef, J.M.; Deuter, M. (1993): Syntaxonomy of Miscanthus x giganteus Greef et Deu. Angewandte Botanik 67, S. 87–90
- Han, D.; Li, W.; Cui, T.; Wang, Q.; Tang, C.; Chen, L.; Qu, Z.; Xu, L. (2024): Biomechanical features and parametric calibration of a bilayer bonded particle model for the cornstalk during harvest. Sci. Rep. 14, 20198, https://doi.org/10.1038/s41598-024-71005-1
- Hertz, H. (1881): Über die Berührung fester elastischer Körper. Journal für die reine und angewandte Mathematik 92, S. 156–171
- Jünemann, D.; Kemper, S.; Frerichs, L. (2013): Prozesssimulation von Halmgut Einsatzmöglichkeiten der Diskrete-Elemente-Methode. Landtechnik 68(3), S. 164–167, https://doi.org/10.15150/lt.2013.221

- Kaack, K.; Schwarz, K.-U. (2001): Morphological and mechanical properties of Miscanthus in relation to harvesting, lodging, and growth conditions. Ind. Crops Prod. 14, pp. 145–154, https://doi.org/10.1016/S0926-6690(01)00078-4
- Kaltschmitt, M.; Hartmann, H.; Hofbauer, H. (2009): Energie aus Biomasse. Springer Berlin, Heidelberg, https://doi.org/10.1007/978-3-540-85095-3
- Kattenstroth, R.; Harms, H.; Lang, Thorsten (2011): Alignment of straw to optimise the cutting process in a combine's straw chopper. Landtechnik 66(5), pp. 354–357, https://doi.org/10.15150/lt.2011.891
- Klein, B. (2021): Versuchsplanung Design of Experiments: Einführung in die Taguchi/Shainin-Methodik. Berlin, de Gruyter, https://doi.org/10.1515/9783110724516
- Kovács, Á.; Kotrocz, K.; Kerényi, Gy. (2015): The adaptability of discrete element method (DEM) in agricultural machine design. Hung. Agric. Eng. pp. 14–19, https://doi.org/10.17676/HAE.2015.27.14
- Kovacs, A.; Radics, J.P.; Kerenyi, G. (2017): A Discrete Element Model For Agricultural Decision Support. In: ECMS 2017 31st Conference on Modelling and Simulation, Ed. Paprika, Z.Z.; Horák, P.; Váradi, K.; Zwierczyk, P.T.; Vidovics-Dancs, A.; Rádics, J.P., pp. 488–494, https://doi.org/10.7148/2017-0488
- Lenaerts, B.; Aertsen, T.; Tijskens, E.; De Ketelaere, B.; Ramon, H.; De Baerdemaeker, J.; Saeys, W. (2014): Simulation of grain-straw separation by Discrete Element Modeling with bendable straw particles. Comput. Electron. Agric. 101, pp. 24–33, https://doi.org/10.1016/j.compag.2013.12.002
- Li, S.; Huan, X.; Wang, T.; Hui, Y.; You, Y.; Wang, D. (2024): Biomechanical properties and discrete element modeling of PSR stalks during silage harvest. Comput. Electron. Agric. 217, 108644, https://doi.org/10.1016/j.compag.2024.108644
- Liu, B.; Koc, A.B. (2017): Mechanical Properties of Switchgrass and Miscanthus. Trans. ASABE 60, pp. 581–590, https://doi.org/10.13031/trans.11925
- Liu, O.; Mathanker, S.K.; Zhang, O.; Hansen, A.C. (2012): Biomechanical Properties of Miscanthus Stems. Trans. ASABE 55, pp. 1125–1131, https://doi.org/10.13031/2013.42231
- Liu, W.; Su, Q.; Fang, M.; Zhang, J.; Zhang, W.; Yu, Z. (2023): Parameters Calibration of Discrete Element Model for Corn Straw Cutting Based on Hertz-Mindlin with Bonding. Appl. Sci. 13, 1156, https://doi.org/10.3390/app13021156
- Meehan, P.G.; McDonnell, K.P.; Finnan, J.M. (2013): An assessment of the effect of harvest time and harvest method on biomass loss for Miscanthus × giganteus. GCB Bioenergy 5, pp. 400–407
- Miao, Z.; Phillips, J.W.; Grift, T.E.; Mathanker, S.K. (2015): Measurement of Mechanical Compressive Properties and Densification Energy Requirement of Miscanthus × giganteus and Switchgrass. BioEnergy Res. 8, pp. 152–164, https://doi.org/10.1007/s12155-014-9495-8
- Mindlin, R.D. (1949): Compliance of Elastic Bodies in Contact. J. Appl. Mech. 16, pp. 259–268, https://doi.org/10.1115/1.4009973
- Mindlin, R.D.; Deresiewicz, H. (1953): Elastic Spheres in Contact Under Varying Oblique Forces. J. Appl. Mech. 20, pp. 327–344, https://doi.org/10.1115/1.4010702
- Potyondy, D.O.; Cundall, P.A. (2004): A bonded-particle model for rock. Int. J. Rock Mech. Min. Sci. 41, pp. 1329–1364, https://doi.org/10.1016/j.ijrmms.2004.09.011
- Sakaguchi, H.; Ozaki, E.; Igarashi, T. (1993): Plugging of the Flow of Granular Materials during the Discharge from a Silo. Int. J. Mod. Phys. B 07, pp. 1949–1963, https://doi.org/10.1142/S0217979293002705
- Siebertz, K.; Van Bebber, D.; Hochkirchen, T. (2017): Statistische Versuchsplanung. Springer Berlin, Heidelberg, https://doi.org/10.1007/978-3-662-55743-3
- Tsuji, Y.; Tanaka, T.; Ishida, T. (1992): Lagrangian numerical simulation of plug flow of cohesionless particles in a horizontal pipe. Powder Technol. 71, pp. 239–250, https://doi.org/10.1016/0032-5910(92)88030-L
- Umweltbundesamt (2025): Erneuerbare Energien in Zahlen. https://www.umweltbundesamt.de/themen/klima-energie/erneuerbare-energien/erneuerbare-energien-in-zahlen#uberblick, accessed on 16 Apr 2025

- Wang, X.; Tian, H.; Xiao, Z.; Zhao, K.; Li, D.; Wang, D. (2024): Numerical Simulation and Experimental Study of Corn Straw Grinding Process Based on Computational Fluid Dynamics-Discrete Element Method. Agriculture 14, 325, https://doi.org/10.3390/agriculture14020325
- Zeng, Z.; Chen, Y. (2019): Simulation of straw movement by discrete element modelling of straw-sweep-soil interaction. Biosyst. Eng. 180, pp. 25–35, https://doi.org/10.1016/j.biosystemseng.2019.01.009
- Zhang, T.; Zhao, M.; Liu, F.; Tian, H.; Wulan, T.; Yue, Y.; Li, D. (2020): A discrete element method model of corn stalk and its mechanical characteristic parameters. BioResources 15, pp. 9337–9350, https://doi.org/10.15376/biores.15.4.9337-9350

#### **Authors**

Niklas Bargen-Herzog, M.Sc., Johannes Knapp, M.Sc., and Benjamin Kazenwadel, M.Sc., are research assistants and Prof. Dr.-Ing. Marcus Geimer is Head of the Institute of Mobile Machines (Mobima) of the Karlsruhe Institute of Technology (KIT), Rintheimer Querallee 2, 76131 Karlsruhe, E-Mail: niklas.bargen-herzog@kit.edu

# Notes and acknowledgements

This research was carried out in the context of the research project "Development of harvesting and logistics technology for the utilization of unused biomass" (Cuboid4Log). The project was funded by the Baden-Württemberg Ministry of Economics, Labor and Tourism as part of the Invest BW program (VwV Invest BW - Innovation II) under the funding code BW1-1075/04.

